IOP Publishing Journal of Physics: Condensed Matter
J. Phys.: Condens. Matter **26** (2014) 255401 (8pp) doi:10.1088/0953-8984/26/25/255401

Helium bubble nucleation and growth in α-Fe: insights from first–principles simulations

W Xiao[1,2,3], X Zhang[2], W T Geng[3], and G Lu[2]

[1] State Key Lab of Nonferrous Metals and Processes, General Research Institute for Nonferrous Metals, Beijing 100088, People's Republic of China
[2] Department of Physics and Astronomy, California State University Northridge, Northridge, California 91330–8268, USA
[3] School of Materials Science and Engineering, University of Science and Technology Beijing, Beijing 100083, People's Republic of China

E-mail: ganglu@csun.edu

Received 7 March 2014, revised 9 April 2014
Accepted for publication 22 April 2014
Published 29 May 2014

Abstract

We have carried out a first-principles study on the nucleation and early-stage growth of He bubbles in Fe. The energetics, atomic and electronic structure of He-vacancy complexes, involving both a monovacancy and a nine-vacancy cluster, are examined. Based on the energetics, we then perform thermodynamics analysis to gain deeper insights into He bubble nucleation and growth. We have determined the energy cost for the nucleation of He bubbles and found that up to eight He atoms can be trapped at a single vacancy. In order to capture more He atoms, the vacancy has to emit Frenkel pairs to release the substantial stress building on the surrounding Fe lattice. Compared to the monovacancy, the nine-vacancy cluster has a lower energy cost for He bubble nucleation and growth. He atoms at the vacancy repel the surrounding electronic charge and redistribute it on the neighboring Fe atoms. The thermodynamic analysis reveals that He chemical potential provides a driving force for He bubble nucleation and growth. There are two critical He chemical potentials that are of particular importance: one of them marks the transition from single He occupation to multiple He occupation at a monovacancy while the other sets off He-induced superabundant vacancy formation.

Keywords: ferritic steels, He bubbles, first-principles, thermodynamics analysis

(Some figures may appear in colour only in the online journal)

1. Introduction

Ferritic steels have emerged as promising candidates for structural materials in future nuclear fusion reactors. Significant research effort has been devoted to understanding the materials behaviors of Fe in extreme environments, such as high temperature, pressure and irradiation [1]. In particular, during the operation of the fusion reactors, a large amount of helium is either directly implanted into or created internally by (n,α) nuclear transmutation reactions in Fe, concurrently with energetic displacement damage, i.e., the formation of vacancies and interstitials. Because of their extremely low solubility in Fe lattice, He atoms have a very strong tendency to bind to vacancies and precipitate into He-vacancy clusters or He bubbles. These He-vacancy clusters can grow further by capturing more and more He and vacancies and ultimately lead to void swelling, blistering, and fatigue fracture that are detrimental to the mechanical properties of the materials [2–6].

He bubble growth is believed to include three stages, characterized by the typical sizes of the He bubbles: early-stage growth of atomistic bubble nucleus (or nucleation of He bubbles), mid-stage growth of non-ideal gas bubbles, and

 © 2014 IOP Publishing Ltd Printed in the UK

late-stage growth of ideal gas bubbles [7–9]. The crucial step of nucleation and early-stage growth involves He_nV_m clusters in the nanometer dimensions and poses unique challenges for illuminating the underlying mechanism. Owing to its atomistic nature, the elucidation of the nucleation and early-stage growth requires more accurate descriptions of atomic interactions beyond empirical formalisms. Unfortunately, such descriptions are often incredibly complex and computationally intensive; thus, they have not been achieved successfully to date. The objective of the present work is to provide a quantum mechanical description for the nucleation and early-stage growth of He bubbles in Fe using first-principles simulations. In particular, we focus on energetics, atomic and electronic structures of He-vacancy clusters. Combining with thermodynamics analysis, we can illustrate the interplay between temperature, He chemical potential, vacancy formation and He-vacancy concentrations. Such analysis provides deeper insights into the atomistic mechanism of He bubble nucleation and illuminates the relationship between He chemical potential and He bubble growth.

Some of the past work that is relevant to this paper is summarized briefly here. For example, based on empirical atomistic simulations, Wilson *et al* have long established that He can bind easily to vacancy clusters, producing vacancies and nearby self-interstitial atoms (SIAs) in metals [10]. A recent first-principles simulation has been performed to interpret and describe He migration in Fe, which is important to the kinetics of He bubble growth [11]. It has been revealed that He atoms prefer to occupy tetrahedral interstitials as opposed to the octahedral interstitials in Fe [12], and these interstitial He could attract each other with a very low migration energy [13]. An unexpected magnetic interaction between Fe and He atoms is discovered by Seletskaia *et al* [14], confirmed by the present work. Based on empirical molecular dynamics (MD) and kinetic Monte Carlo simulations, Morishita *et al* [15] have demonstrated that the growth and shrinkage of He-vacancy clusters strongly depends on He density in line with our findings. A first-principles simulation has been carried out to examine the stability of small He-vacancy clusters [16] and a further empirical MD study has explored larger clusters with m up to 15 and n up to $5m$ [17]. With empirical MD simulations, Gao *et al* [18] have studied the atomic structure of He_nV_1 clusters at room temperature. They discovered that when $n \geqslant 16$, the He_nV_2 cluster is stabilized by the emission of an SIA in the form of a <1 1 0> dumbbell. Finally, the work by Ismer *et al* [19] on hydrogen in Al has motivated the thermodynamics analysis in the present work.

2. Computational details

Defect formation energies are the key to understanding He bubble nucleation and growth in Fe. Here we focus on the formation energy of He-defect complexes (vacancies or interstitials) under conditions of zero pressure and constant volume as defined in the following:

$$E_P(r\mathrm{Fe},\, s\mathrm{He}) = E_P^{tot}(r\mathrm{Fe},\, s\mathrm{He}) - r\mu_{Fe} - s\mu_{He}, \qquad (1)$$

or

$$E_V(r\mathrm{Fe},\, s\mathrm{He}) = E_V^{tot}(r\mathrm{Fe},\, s\mathrm{He}) - r\mu_{Fe} - s\mu_{He}, \qquad (2)$$

where r and s are the numbers of Fe and He atoms in the supercell, respectively. Subscript P or V denotes the energy calculated under the condition of constant pressure or constant volume. $E_P(r\mathrm{Fe}, s\mathrm{He})$ and $E_P^{tot}(r\mathrm{Fe}, s\mathrm{He})$ represent He-defect formation energy and the total energy of the supercell under the zero pressure condition, respectively. There is a similiar definition for the corresponding quantities under the constant volume condition. μ_{Fe} and μ_{He} are the chemical potential of Fe and He, respectively. Here, μ_{Fe} is defined as the total energy per atom in a perfect Fe lattice at zero temperature calculated by $\mu_{Fe} = \dfrac{E_{bulk}^{tot}(128\mathrm{Fe})}{128}$. E_{bulk}^{tot} is the total energy of the supercell consisting 128 Fe atoms in the perfect bcc lattice. 128 Fe atoms as opposed to a single Fe atom are used in the periodic calculations to minimize possible numerical errors. The chemical potential of He is defined as $\mu_{He} = \mu_{He}^0 + \Delta\mu_{He}$, where μ_{He}^0 is the chemical potential of an isolated He atom in vacuum at T= 0 K. $\Delta\mu_{He}$ represents the chemical potential contribution due to the environment such as temperature and concentration of implanted He. $\Delta\mu_{He}$ is very difficult to assess from first-principles and we will make no attempt to do so. Instead, we will simply calculate physical quantities as a function of μ_{He} to establish general trends, without specifying the experimental conditions for realizing such chemical potentials.

The thermodynamics of He bubble growth depends on the concentration of He-vacancy clusters. Assuming the dilute limit of the defects, we can calculate the equilibrium concentration of the defects at temperature T as follows: [19, 20]

$$c = N_{config}\exp\left(-\frac{E_P}{k_B T}\right), \qquad (3)$$

where N_{config} is the number of equivalent defect configurations per lattice site and k_B is the Boltzmann constant. We have estimated the free energy contribution due to the vibrational entropy of He at 900 K, which is one order of magnitude smaller than the He formation energy at a vacancy and thus can be neglected.

The total energies are computed based on density functional theory (DFT) with plane-wave basis and pseudopotentials as implemented in Vienna *Ab initio* Simulation Package (VASP) [22, 23]. The projector augmented wave method is used for treating pseudopotentials [24, 25] and the exchange-correlation (XC) interaction is described by generalized gradient approximation in Perdew–Burke–Ernzerhof (PBE) form [26]. Unless otherwise stated, all calculations are carried out in a supercell of $4a_0 \times 4a_0 \times 4a_0$ (with 128 Fe atoms for a perfect lattice), where a_0 is the lattice constant of Fe. A $(3 \times 3 \times 3)$ k-point mesh within Monkhorst–Pack scheme and an energy cutoff of 480 eV are used in the calculations.

3. Results and discussions

First, we briefly compare the formation energies of typical point-defects with related results in literature. As shown in

Table 1. The formation energy of typical point-defects in Fe at zero pressure E_P (eV). The volume changes of the computational supercell are listed as well as related results from literature.

		octa	tetra	sub	Vacancy	Divacancy	SIA
This work	E_P	4.74	4.54	4.39	2.17	4.18	3.90
	ΔV (%)	0.77	0.76	0.08	–0.13	–0.25	1.48
[12]	E_P	4.75	4.56	4.34	2.14		
[14]	E_P	4.60	4.37	4.08			
[13]	E_P	4.57	4.39	4.22			
[21]	E_P				2.02		3.94

table 1, there is a very good agreement between our results and those of Zu *et al* [12], both based on VASP calculations. The minor differences are due to different energy cutoffs (480 ev versus 500 ev) and different XC functionals (PBE versus PW91 [27]) in the respective calculations. Also using VASP with an energy cutoff of 300 ev and the XC functional of PW91, Seletskaia *et al* [14] obtained somewhat lower formation energies. The calculations of Fu *et al* employed a real-space DFT code, SIESTA, and yielded results between ours and those of Seletskaia *et al* The disparity in the defect energies reflects the computational challenges as alluded to earlier. Qualitatively, however, these DFT calculations all yield the same ranking of the defect formation energies; namely, the substitutional site (sub) is the least endothermic (or the most stable) among the three, and between the interstitial sites, He prefers the tetrahedral site (tetra) to the octahedral site (octa).

Constant bombardment by high energy neutrons produces a large number of He atoms in Fe matrix. These He atoms can move easily between the interstitials thanks to the small migration barrier (0.06 ev) of He [13]. The much higher energies at the tetra and octa interstitials comparing to the vacancy formation energy underlies the prevalence of He-vacancy clusters in Fe. For example, the energy gain as a tetrahedral He atom is trapped by a vacancy is given by: E_P(tetra) $-(E_P$(sub)$-E_P$(vac)) = 4.54 ev -2.22 ev = 2.32 ev.

Although the likelihood of large vacancy cluster formation is very small, they can nonetheless exist and trap multiple He atoms under high irradiation. Hence in this work, we will consider two representative vacancy configurations, a dominant case with a monovacancy ($n = 1$) and a less probable case with a nine-vacancy-cluster ($n = 9$).

3.1. Energetics of He-vacancy clusters

3.1.1. He-monovacancy clusters. In this section, we focus on the energetics of He-vacancy clusters at 0 K with $\mu_{He} = 0$. We have calculated the formation energies of various He_nV_1 clusters with n ranging from 1 to 12—each with n He atoms occupying a monovacancy. Gao *et al* [18] have previously studied the atomic structures of He_nV_1 clusters using empirical MD simulations and found symmetric arrangements of He atoms until $n = 9$. Hence, we compute the formation energies of the clusters based on the symmetric arrangements of He atoms; some of them are displayed in figure 1 for $n = 2$, 6 and 9. For a smaller cluster ($n = 2 \sim 6$), the volume expansion of the surrounding Fe lattice is smaller; however, when the cluster grows

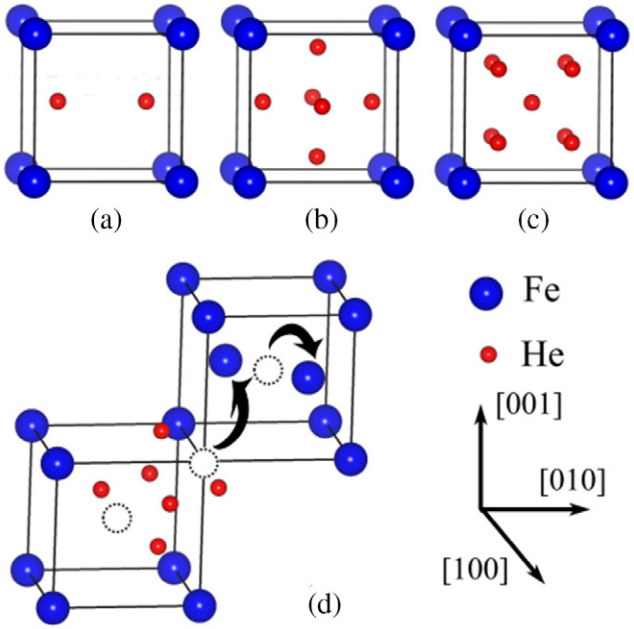

Figure 1. (*a–c*) The atomic configurations of He_nV_1 clusters ($n = 2$, 6 and 9) and (*d*) a schematic diagram of a Frenkel pair in $He_6V_2I_1$ cluster. Blue and red spheres represent Fe and He atoms, respectively. Dashed circle indicates a vacancy.

larger (e.g., $n = 9$), a significant volume expansion is observed and the interatomic distances between the first-shell Fe atoms surrounding He increase 28% . This expansion could produce a pressure imposed by the He bubble onto the surrounding Fe lattice. Of course, at remote distances from the He bubble, the pressure is faded away. In figure 2, we show the formation energies of the He-vacancy clusters under zero pressure in black symbols. We find that the formation energy increases monotonically with the number of He atoms, consistent with the previous MD results [18]. In particular, for smaller clusters ($n = 1 \sim 6$), the energy increase is linear with a slope of 2.72 ev/atom. This slope represents the energy penalty rate for the growth of small bubbles. When more He atoms are trapped ($n > 6$), the energy increase deviates slightly from the straight-line. We have explored several high-symmetry orientations for He dumbbells in each cluster and found their energy differences to be generally small. For example, the energy differences for a He_2 dumbbell orientated along $\langle 1\,0\,0\rangle$, $\langle 1\,1\,0\rangle$ and $\langle 1\,1\,1\rangle$ directions in He_2V_1 cluster are less than 0.04 ev.

With a continuous accumulation of He at the vacancy, a significant pressure builds up on the surrounding Fe lattice. There are two plausible mechanisms to release the pressure: the emission of a He at an interstitial or kick-out of a Frenkel pair (vacancy plus a nearby SIA). For the first mechanism, the energy cost for emitting a He atom at the tetrahedral site is 4.54 ev. This energy should be contrasted to the energy cost for the growth of the He cluster, which is 2.72 ev per He atom. Hence it is energetically forbidden to emit an interstitial He. This can also be seen more formally by calculating the trapping energy of He at a vacancy [19],

$$E^{\text{trap}}(n) = E_P(\text{v}+n\text{He}) - \{E_P[\text{v}+(n-1)\,\text{He}] + E_P(\text{tetra})\}\,. \quad (4)$$

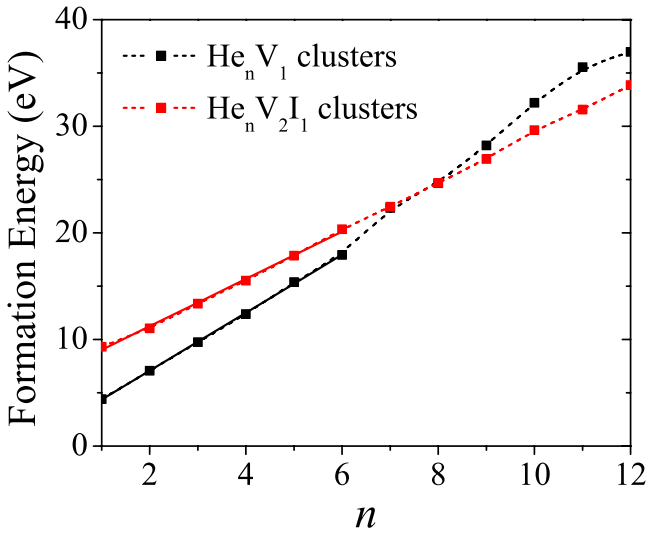

Figure 2. The formation energies at zero pressure E_P (eV) of He_nV_1 and $He_nV_2I_1$ clusters as a function of n. A linear fit to E_P between $n = 1 \sim 6$ is also displayed.

Because the difference between the first two terms represents the slope of figure 2 (2.72 ev), lower than E_P(tetra), $E^{trap}(n)$ is always negative for $n = 1 \sim 12$. In contrast, the kick-out of a Frenkel pair (labeled by $He_nV_2I_1$) is energetically viable and is examined in the following. The atomic structure of the Frenkel pair is shown schematically in figure 1(*d*) with 6 He atoms as example. At the center of the lower cube resides the original vacancy; one of its nearest neighbor Fe atoms (the open circle) is displaced to form an SIA in the upper cube indicated by an arrow. At the same time, the center Fe in the upper cube is also pushed aside, leaving behind a vacancy (open circle). As a result, a ⟨1 1 1⟩ di-vacancy and a ⟨1 1 0⟩ dumbbell (two SIAs) are created next to the original vacancy. The He atoms at the vacancy have shifted towards the di-vacancy in a symmetrical manner. It is shown that the He-free Frenkel pair V_2I_1 is energetically unstable and there is no barrier for it transforming to the stable structure V_1. However, even with only one He atom, the Frenkel pair $He_1V_2I_1$ is stabilized although its formation energy is still much higher than that of He_1V_1. In figure 2, the formation energies of $He_nV_2I_1$ clusters involving a Frenkel pair are shown in red symbols. The formation energies can also be approximated by a straight-line with a slope of 2.22 ev/atom, smaller than that of He_nV_1 clusters.

As n increases, the Frenkel pair becomes more and more stable. At $n = 8$, the two straight-lines cross and the cluster with a Frenkel pair is more stable than that with a vacancy; the kick-out mechanism starts operating for larger He-vacancy clusters. Hence the initial growth of He bubbles could be described as follows: monovacancies are dominant defects for He bubble nucleation and growth. For a smaller cluster with $n \leqslant 6$, He occupies the vacancy symmetrically with less lattice expansion and pressure; the He cluster grows at a energy cost of 2.72 ev/atom. As the He cluster grows to $n = 6$, the surrounding Fe lattice is significantly deformed and the energy cost for further growth is increased. Once n reaches 9, the pressure is large enough to kick out a Frenkel pair which lowers the energy cost (2.22 ev/atom) for bubble growth until $n = 12$. Beyond $n = 12$, more Frenkel pairs would be emitted to lower the energy [28]. We find that at most 8 He atoms can be trapped by a monovacancy, which is at odds to Gao *et al* [18] who claimed that up to 15 He atoms can be held in a monovacancy. They arrived at this conclusion by comparing the energy of He_nV_1 to that of He_nV_2 plus an isolated SIA *far-away* from the vacancy. By contrast, we compare the same energy to that of He_nV_2 plus a *nearby* SIA, i.e., $He_nV_2I_1$. Although it is known that a long-range interaction between a He bubble and SIA is repulsive from an elasticity point of view (the elastic interaction between two dilation centers is repulsive), their short-range interaction is dominated by chemical interactions such as charge redistributions, which should be treated quantum mechanically. In fact, our first-principles simulations suggest that the short-range interaction between the He bubble and SIA is actually attractive, and there is a large energy release when a far-away SIA approaches the He_nV_2 cluster. By calculating the energy difference between $He_nV_2I_1$ (with the nearby SIA) and He_nV_2 plus an isolated SIA, we find the energy release as 0.63 ev and 0.98 ev for $n = 6$ and 8, respectively. Since the SIA is more likely to be generated near the original vacancy, such short-range attraction could stabilize the SIA in the proximity of the He bubble. In addition, the energy release is greater for a larger cluster, supporting the volume diffusion mechanism of He bubble growth [29] where He bubbles, especially in large sizes, could move through Fe lattice adsorbing vacancies and SIAs.

3.1.2. He-nine-vacancy clusters. Next we study the energetics of He in a nine-vacancy cluster by removing one Fe atom and its eight nearest neighbors. A supercell of $5a_0 \times 5a_0 \times 5a_0$ (with 250 atoms) is employed to simulate the nine-vacancy cluster. The Brillouin zone is sampled by $2 \times 2 \times 2$ k-point mesh. A perfect bcc supercell, containing 250 Fe atoms, is used as a reference in the calculation of Fe chemical potential, μ_{Fe}. Six He-vacancy clusters are considered in the calculations, including 1 He atom at the center of the vacancy complex, a dumbbell of 2 He atoms at the center, 6 He atoms (one on each face-center), 9 He atoms (each occupying a vacancy site), 15 He atoms consisted of 6 face-centers and 9 vacancy sites, and 35 He atoms with 9 at vacancy sites and the remaining atoms surrounding these atoms symmetrically.

The formation energies (E_P) of He_nV_9 clusters as a function of n under zero pressure is shown in figure 3 in black symbols. The formation energy increases monotonically and can be represented by two straight lines with different slopes. For $n < 10$, the slope is 1.10 ev/atom and for $10 < n < 35$, the slope is 1.74 ev/atom. With more He trapped to the vacancy cluster, the lattice expansion becomes larger, hence a steeper energy increase. Note that both slopes are smaller than that of He_nV_1 due to the larger volume available in the 9-vacancy cluster. For $He_{35}V_9$, there is a significant expansion in the first-shell of Fe atoms surrounding the He bubble, and the corresponding interatomic distances between the first-shell Fe atoms surrounding He increase 36% . Similar to the case in monovacancy, a kick-out of Frenkel pair is expected to occur under this stress.

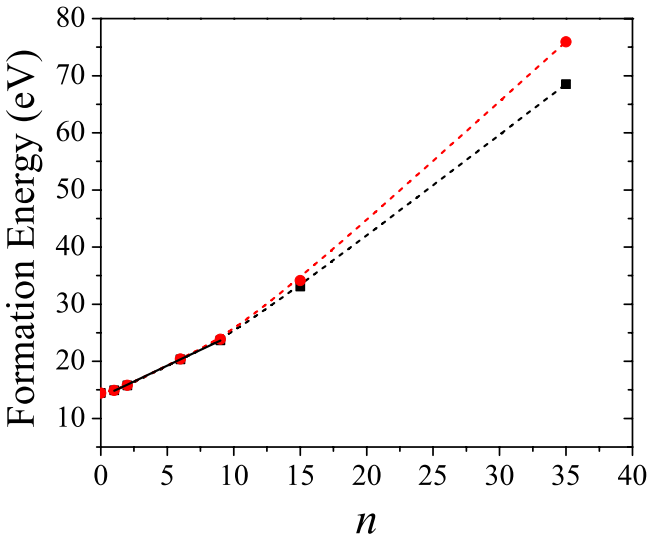

Figure 3. The formation energies at zero pressure E_P (eV) (black dashed line) and under a constant volume E_V (eV) (red dashed line) of He_nV_9 clusters as a function of n.

We have also calculated the formation energies (E_V) of He_nV_9 clusters as a function of n under a constant volume (equilibrium volume at 0 K) shown in figure 3 in red symbols. For $n < 9$, because the volume expansion is negligible, E_V is almost identical to E_P. When the He bubble grows larger, E_V is increasingly higher than E_P. For $n > 15$, the volume expansion is so large that the constant pressure calculation is a must.

3.2. Electronic structure of He-vacancy clusters

To elucidate the electronic structure of He-vacancy clusters, we calculate He-induced charge density redistribution which is defined as the difference between the total charge density of He_nV_1 cluster and the partial charge density of the He-free vacancy cluster plus the charge density of He atoms. The positive (negative) charge density indicates charge accumulation (depletion) upon the introduction of He atoms into the vacancy. We find that the He atoms repel the surrounding charge cloud, forming a charge-depletion shell around them (there is also minor charge transfer onto the He atoms). The spilled-out charge redistributes on the neighboring Fe atoms. The directional d bonding between Fe atoms is clearly visible while the charge density on He is spherical (red circles), indicative of the inert nature of He.

The local density of states (DOSs) for two representative clusters He_1V_1 and He_2V_1 are displayed in figures 4(*b*) and (*c*). The s- and p-projected DOS of a He atom is shown in the lower panel whereas the d-projected DOS on one of its the nearest neighbor Fe atoms is shown in the upper panel. For both clusters, there is 3d-2s hybridization between Fe and He, but 2p DOS on the He atom is negligible. The d-DOS on Fe is similar for the two clusters, suggesting that the electronic structure of Fe is not sensitive to the nearby He atom. We find that 2s-electron of He in He_2V_1 cluster is spin-polarized by Fe as shown in figure 4(*c*). The He–He interaction in He_2V_1 broadens the s-DOS, merging the two DOS peaks of He_1V_1 into one. On the contrary, there is no magnetic moment on He atom in He_1V_1, consistent with the result of Seletskaia *et al* [14].

3.3. Thermodynamics of He-vacancy clusters

To perform thermodynamic analysis of the *early*-stage growth of He bubbles, we assume that He only occupies monovacancies and interstitials in light of their formation energies. For example, a ⟨1 1 1⟩ divacancy and the nine-vacancy has a formation energy of 4.18 ev and 14.46 ev, respectively, much higher than that of monovacancy and interstitial. Although a larger vacancy cluster can lower its formation energy by incorporating He atoms [16], it is still energetically more costly than a monovacancy when the number of incorporated He atoms is small (< 8). Therefore we can ignore the contributions of larger vacancy clusters to the early-stage growth of He bubbles.

The total vacancy concentration in equilibrium c_v^{tot} is composed of two contributions: the concentration of He-free vacancies c_v^0 and the concentration of He-containing vacancies c_v^{He}. Thus $c_v^{tot} = c_v^0 + c_v^{He}$, where $c_v^0 = \exp\left[-\frac{E_v^0}{k_B T}\right]$ and E_v^0 is the vacancy formation energy in He-free material independent of He chemical potential μ_{He}. c_v^{He} can be calculated by

$$c_v^{He} = \sum_{n=1}^{n^{max}} S(n) \exp\left[-\frac{E_P(v+n\mathrm{He}, \mu_{He})}{k_B T}\right]. \quad (5)$$

Here n^{max} is the maximum number of He atoms in a monovacancy before kicking out the Frenkel pair and $n^{max} = 8$. $S(n)$ denotes the number of distinct configurations of n He occupying the monovacancy, which can be evaluated approximately by $\frac{n^{max}!}{n!(n^{max}-n)!}$ [19]. These positions of He occupation at the vacancy are energetically stable and thus countable for a statistical analysis. The approximation has been successfully used for studying the thermodynamics of H occupying vacancies in Al and Mg based on first-principles calculations [19]. $E_P(v+n\mathrm{He}, \mu_{He})$ is the formation energy of He_nV_1 cluster under zero pressure. Therefore, c_v^{He} represents the concentration of He-induced vacancies. The He chemical potential μ_{He} should be greater than that in vacuum (i.e., zero). Since μ_{He} represents the average energy of He atoms in Fe, it should be less than the formation energy of He at the octahedral site (4.74 ev). Therefore, in the following discussion, we let μ_{He} vary in the interval of [0, 5] ev.

Similarly, the total He concentration c_{He}^{tot} is assumed to include only two contributions, c_{He}^0 and c_{He}^v. c_{He}^0 represents He concentration at the tetrahedral interstitials, and c_{He}^v denotes He concentration at vacancies. Since there are six equivalent tetrahedral interstitials per Fe lattice site, $c_{He}^0 = 6\exp\left[-\frac{E_P(\mathrm{tetra}, \mu_{He})}{k_B T}\right]$ where $E_P(\mathrm{tetra}, \mu_{He})$ is the formation energy of a He at the tetrahedral site under zero pressure. c_{He}^v can be evaluated similarly as equation (5):

$$c_{He}^v = \sum_{n=1}^{n^{max}} nS(n) \exp\left[-\frac{E_P(v+n\mathrm{He}, \mu_{He})}{k_B T}\right]. \quad (6)$$

The logarithm concentrations of monovacancies and He as a function of μ_{He} are shown in figures 5(*a*) and (*b*), respectively.

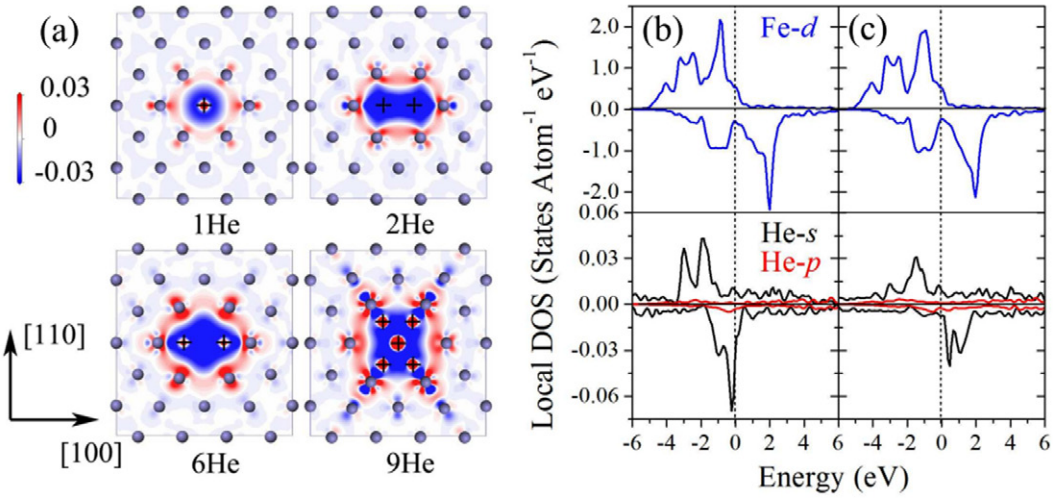

Figure 4. (*a*) He-induced charge density redistribution in (1 1 0) plane for He_nV_1 clusters (n = 1, 2, 6 and 9). Red and blue color in the contour plot represents charge accumulation and depletion, respectively as He is introduced into the vacancy. He and Fe atoms on the (1 1 0) plane are indicated by the cross and blue spheres, respectively. (*b*) Local DOS for the He atom and its nearest neighbor Fe atom in He_1V_1(*b*) and He_2V_1(*c*) clusters. Spin-up and spin-down DOS are given in positive and negative values, respectively. The blue, black and red curves represent Fe-d, He-s and He-p local DOS, respectively. The Fermi energy is at 0 ev.

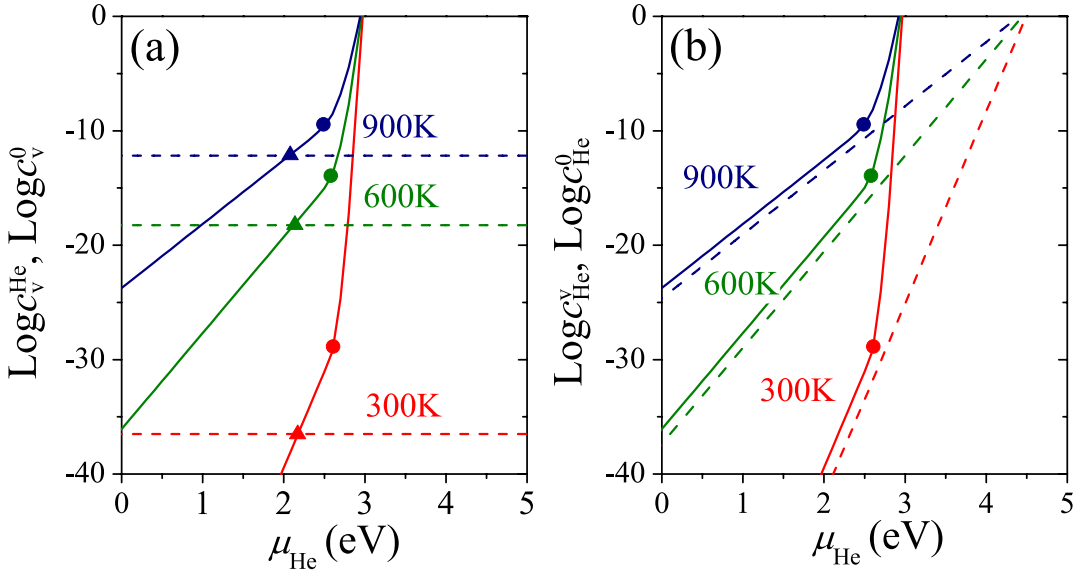

Figure 5. Concentration in logarithm as a function of He chemical potential μ_{He} at different temperatures, T = 300 K (red), 600 K (green) and 900 K (blue). (*a*) Vacancy concentration containing He (solid lines) and He-free vacancy concentration (dashed lines). (*b*) He concentration in vacancies (solid lines) and He concentration at the tetrahedral interstitials (dashed lines).

In figure 5(*a*), at each T, the concentration of He-containing vacancies c_v^{He} increases exponentially as a function of μ_{He} whereas the He-free vacancy concentration c_v^0 remains a constant indicated by the horizontal dashed line. The intersections between c_v^0 and c_v^{He}, labeled by triangles and denoted by μ_{He}^{in}, are 2.16 ev at 300 K, 2.14 ev at 600 K and 2.09 ev at 900 K. At each T, there is a sharp transition at a critical He chemical potential, μ_{He}^c, indicated by a solid circle, beyond which c_v^{He} increases rapidly. μ_{He}^c is 2.61 ev at 300 K, 2.58 ev at 600 K and 2.49 ev at 900 K. It turns out that this sharp rise is due to multiple He atoms occupying a single vacancy (or multiple He occupation). When μ_{He} is low, there are few He atoms in Fe, hence He-occupied vacancy concentration c_v^{He} is much lower than c_v^0. As more and more He are present and μ_{He} increases, a large amount of He-containing vacancies are generated. Once μ_{He} reaches μ_{He}^{in}, the concentration of He-occupied vacancies exceeds that of He-free vacancies, leading to so-called He-induced superabundant vacancy formation. As even more He atoms are injected into Fe with $\mu_{He} > \mu_{He}^c$, the multiple He occupation kicks in, and c_v^{He} increases drastically. We will elaborate on the origin of this sharp increase later.

Similarly, at each T He concentrations in Fe, including both at vacancies and the interstitials, also increase exponentially with μ_{He} as shown in figure 5(*b*). As mentioned above, there is a direct correspondence between μ_{He} and the number of He atoms in the material; the higher the He chemical potential, the more the He atoms are present in the material. We find that when $\mu_{He} < \mu_{He}^c$, He concentration at vacancies is more than an

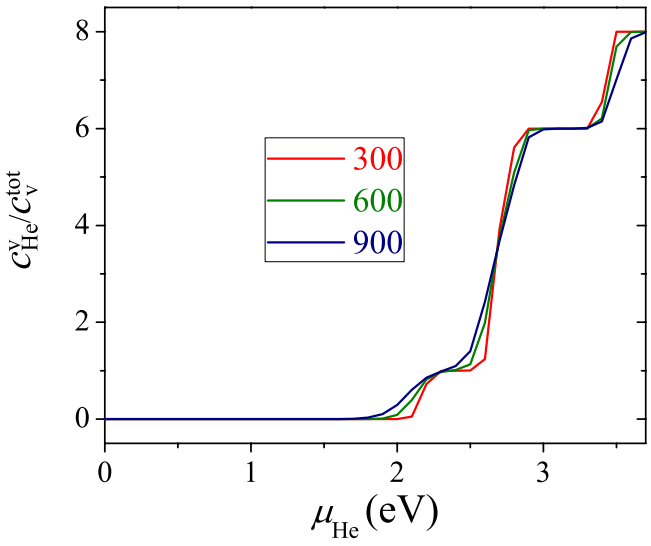

Figure 6. Average number of He atoms trapped in monovacancies calculated by c_{He}^{v} / c_{v}^{tot} at different temperatures, T = 300 K (red), 600 K (green) and 900 K (blue).

order of magnitude higher than that at the interstitials. There are also sharp transitions of c_{He}^{v} (solid lines) at the same critical He chemical potentials as μ_{He}^{c} ; this is because c_{He}^{v} and c_{v}^{He} are related by a factor of n. As more and more He atoms are present with $\mu_{He} > \mu_{He}^{c}$, the ratio c_{He}^{v} / c_{He}^{0} explodes. This explosion is due to the surge of He-induced vacancies, set off by the multiple He occupation. In contrast, there is no such transition for He at the interstitials as no more than one He atom can occupy each interstitial.

One can also estimate μ_{He}^{c} and μ_{He}^{in} from the energetics directly. μ_{He}^{in} represents the He chemical potential when the He-free vacancy concentration equals to the He-containing vacancy concentration. The latter can be approximated by the vacancy concentration containing one He atom. Thus μ_{He}^{in} is determined by solving the equation $E_P(\text{v+He}, \mu_{He}^{in}) = E_P(\text{v})$, yielding $\mu_{He}^{in} = 2.22$ ev. Another way to understand this is following: vacancies are being formed and destroyed spontaneously due to thermal fluctuations. If a He atom possesses enough energy, it can combine with a nearby vacancy that is being formed. The energy required for the He atom should thus be the energy difference between the He substitutional energy (4.39 ev) and the vacancy formation energy (2.17 ev). Therefore, μ_{He}^{in} provides such required energy for He, which is 2.22 ev. μ_{He}^{c} marks the transition point where multiple He atoms start occupying a single vacancy, and it can be calculated by the equation $E_P(\text{v}+n\text{He}, \mu_{He}^{c}) = E_P(\text{v+He}, \mu_{He}^{c})$. Thus μ_{He}^{c} should equal to the slope of the black line in figure 2, 2.72 ev.

In figure 6, we plot the ratio c_{He}^{v} / c_{v}^{tot}, the average number of He atoms trapped at each vacancy. As μ_{He} is small, few He atoms are present in the material, thus vacancies are unoccupied on average. When $\mu_{He} > \mu_{He}^{in} = 2.22$ ev, each vacancy is occupied by one He atom. When $\mu_{He} > \mu_{He}^{c} = 2.72$ ev, multiple He atoms are trapped at each vacancy. In fact, up to six He atoms can be accommodated at each vacancy with only a minor increase of He chemical potential. Beyond six He atoms, an extra chemical potential ($\sim$ 0.5 ev) is required for further growth of the He bubble indicated by the step in figure 6. The maximum number of He atoms trapped in each vacancy is eight. When $n > 8$, the kick-off of Frenkel pairs would operate, beyond the premise of our thermodynamics analysis. Once $\mu_{He} > \mu_{He}^{c}$, the probability of creating various He bubbles $He_nV_1 (n = 1 \sim 6)$ is the same, because the energy costs for their formation are the same (2.72 ev) and can be provided by μ_{He}. In other words, many more He bubbles with different sizes from n = 1–6 can be formed simultaneously. Therefore, the extra energy $\mu_{He} - \mu_{He}^{c}$ carried by each He can add up and be harvested to trigger the formation of more vacancies. In other words, multiple He occupation can effectively reduce the vacancy formation energy, giving rise to the sharp increase of c_{v}^{He} as shown in figure 5(*a*). By contrast, for $\mu_{He}^{in} < \mu_{He} < \mu_{He}^{c}$, the extra energy of only *one* He atom can be harvested, thus the concentration of vacancies is much lower. Finally as shown in figure 5(*b*), at μ_{He}^{c}, c_{He}^{0} is in the order of 10^{-10} for 900 K, and 10^{-30} for 300 K, respectively. Even at such low interstitial He concentrations, multiple He atoms can be trapped at single vacancies, which is an indication that Fe is susceptible to He bubble nucleation and growth [30].

4. Conclusions

In summary, we have studied the energetics, atomic and electronic structure of He-vacancy clusters in Fe using first-principles calculations. Based on the energetics, we perform thermodynamics analysis to provide deeper insights on the nucleation and early-stage growth of He bubbles. We have determined the energy costs for the nucleation of He bubbles and found that up to eight He atoms can be trapped at a single vacancy. In order to capture more He atoms, the vacancy has to emit Frenkel pairs to release the substantial stress on the surrounding Fe lattice. The He atoms at the vacancy repel the surrounding electronic charge and redistribute it on the neighboring Fe atoms. The electronic hybridization between He 2s states and Fe 3d states is developed. The thermodynamic analysis reveals that He chemical potential provides a driving force for He bubble nucleation and growth. There are two critical He chemical potentials, μ_{He}^{c} and μ_{He}^{in} that are of particular importance. The former marks the transition from the single He occupation to the multiple He occupation at a monovacancy while the latter sets off the He-induced superabundant vacancy formation.

Acknowledgments

The work at California State University Northridge was supported by the Office of Naval Research. WX and WTG thank the support by MOST of China (grant no. 2011GB108002).

References

[1] Bloom E E 1998 *J. Nucl. Mater.* **258–63** 7
[2] Chen J, Jung P, Hoffelner W and Ullmaier H 2008 *Acta Mater.* **56** 250

[3] Feldmann G, Fichtner P F P and Zawislak F C 2004 *Acta Mater.* **52** 693
[4] Chen J, He Z Y and Jung P 2006 *Acta Mater.* **54** 1607
[5] Blaschko O, Pleschiutschnig J, Glas R and Weinzierl P 1991 *Phys. Rev.* B **44** 9164
[6] Amarendra G, Viswanathan B, Bharathi A and Gopinathan K P 1992 *Phys. Rev.* B **45** 10231
[7] Trinkaus H 1983 *Radiat. Eff.* **78** 189
[8] Hao W and Geng W T 2012 *Nucl. Instrum. Methods Phys. Res. Sect.* B **280** 22
[9] Hao W and Geng W T 2012 *J. Phys.: Condens. Mater.* **24** 095009
[10] Wilson W D, Bisson C L and Baskes M I 1981 *Phys. Rev.* B **24** 5616
[11] Samaras M 2009 *Mater. Today* **12** 46
[12] Zu X T, Yang L, Gao F, Peng S M, Heinisch H L, Long X G and Kurtz R J 2009 *Phys. Rev.* B **80** 054104
[13] Fu C C and Willaime F 2005 *Phys. Rev.* B **72** 064117
[14] Seletskaia T, Osetsky Y, Stoller R E and Stocks G M 2005 *Phys. Rev. Lett.* **94** 046403
[15] Morishita K, Sugano R, Wirth B D and Diaz de la Rubia T 2003 *Nucl. Instrum. Methods Phys. Res. Sect.* B **202** 76
[16] Fu C C and Willaime F 2007 *J. Nucl. Mater.* **367–70** 244
[17] Lucas G and Schaublin R 2009 *J. Nucl. Mater.* **386–8** 360
[18] Gao N, Victoria M, Chen J and Van Swygenhoven H 2011 *J. Phys.: Condens. Mater.* **23** 245403
[19] Ismer L, Park M S, Janotti A and Van de Walle C G 2009 *Phys. Rev.* B **80** 184110
[20] Van de Walle C G and Neugebauer J 2004 *J. Appl. Phys.* **95** 3851
[21] Domain C and Becquart C S 2001 *Phys. Rev.* B **65** 024103
[22] Kresse G and Furthmuller J 1996 *Comput. Mater. Sci.* **6** 15
[23] Kresse G and Furthmuller J 1996 *Phys. Rev.* B **54** 11169
[24] Blochl P E 1994 *Phys. Rev.* B **50** 17953
[25] Kresse G and Joubert D 1999 *Phys. Rev.* B **59** 1758
[26] Perdew J P, Burke K and Ernzerhof M 1996 *Phys. Rev. Lett.* **77** 3865
[27] Perdew J P, Chevary J A, Vosko S H, Jackson K A, Pederson M R, Singh D J and Fiolhais C 1992 *Phys. Rev.* B **46** 6671
[28] Gao N, Van Swygenhoven H, Victoria M and Chen J 2011 *J. Phys.: Condens. Mater.* **23** 442201
[29] Morishita K and Sugano R 2007 *Nucl. Instrum. Methods Phys. Res. Sect.* B **255** 52
[30] Ishizaki T, Xu Q, Yoshiie T, Nagata S and Troev T 2002 *J. Nucl. Mater.* **307–11** 961